The HKU Scholars Hub The University of Hong Kong 香港大學學術庫

Title	Smart distribution network device for microgrid applications
Author(s)	Tan, KT; So, PL; Chu, YC; Chen, MZ
Citation	The IEEE 15th International Conference on Harmonics and Quality of Power (ICHQP 2012) Hong Kong, 17-20 June 2012. In Conference Proceedings, 2012, p. 842-847
Issued Date	2012
URL	http://hdl.handle.net/10722/160292
Rights	International Conference on Harmonics and Quality of Power Proceedings. Copyright © IEEE.

Smart Distribution Network Device for Microgrid Applications

K. T. Tan, *Student Member, IEEE*, P. L. So, *Senior Member, IEEE*, Y. C. Chu, *Senior Member, IEEE,* and M. Z. Q. Chen, *Member, IEEE*

***Abstract*--This paper focuses on the design of a smart distribution network device for improving the power quality and reliability of the overall power distribution system that the microgrid is connected to. The control design employs a newly developed Model Predictive Control algorithm which optimizes the steady-state and the transient control problems separately to achieve a faster computational time for large power systems. Kalman filters are also employed as state observers to identify the required signals needed for monitoring purposes as well as to extract the harmonic spectra of the grid voltage and the load currents. The design concept is verified through different test case scenarios to demonstrate the capability of the proposed device and the results obtained are discussed.**

***Index Terms*--Power quality, model predictive control, Kalman filters, microgrid.**

I. Introduction

THE concept of microgrid has become a promising alternative for traditional power distribution system for its capability to offer consumers with increased reliability and reduction in total energy losses [1], [2]. However, the connection of a microgrid to the distribution grid poses several power quality (PQ) problems on the performance of the overall power system. These PQ problems include harmonic distortion, voltage and frequency deviations in the grid voltage, and harmonic distortion in the load currents.

To overcome the aforementioned PQ problems, different power-conditioning devices such as active filters [3]–[5], uninterruptible power supplies [6]–[8], dynamic voltage restorers [9]–[10] and unified power quality conditioners [11] are usually employed by customers to protect their loads and systems against PQ disturbances in the distribution network. However, these devices are usually installed at the customers' side and the PQ problems that they are capable to handle are usually limited.

In what follows, this paper provides a comprehensive solution for the operation of a smart distribution network device to tackle a wide range of PQ issues for a microgrid. The device is realized using a combination of series and shunt voltage source inverters (VSI) and is installed at the point of common coupling (PCC) of the distribution grid that the microgrid and other electrical networks are connected to. The proposed controller is a newly developed Model Predictive Control (MPC) algorithm to track periodic reference signals for fast sampling linear time-invariant (LTI) systems that are subject to input constraints. This control methodology decomposes the control problem into steady-state and transient sub-problems which are optimized separately. In this way, the computational time is greatly reduced.

II. System Description

Fig. 1 shows the configuration of the microgrid proposed in this paper for implementation of the smart distribution network device. The proposed microgrid consists of three radial feeders (1, 2 and 3) where feeders 1 and 3 are each connected to a DG unit consisting of a microgenerator, a three-phase VSI, a three-phase LC filter and a local load. Feeder 2, however, is connected directly to an electrical load. The load types in the microgrid will be discussed in Section V.

The device is operated in two modes: (1) PQ compensation and (2) emergency operation. During grid-connected operation, the microgrid is connected to the distribution grid at the PCC. The two DG units are controlled to provide local power and voltage support for loads 1, 2 and 3, and hence reduce the burden of generation and delivery of power directly from the utility grid. The device functions to compensate for any harmonics in the currents drawn by the nonlinear loads in the microgrid so that the harmonics will not propagate to the rest of the electrical networks that are connected to the PCC. The device also functions to compensate for harmonics in the grid voltage which are caused by other nonlinear loads that are connected at the PCC. The device is also equipped with the capability to handle voltage variations in the grid voltage which are caused by the energization of large loads and rapid changes in the load demand.

When a fault occurs on the upstream network of the grid, the circuit breakers (CBs) operate to disconnect the microgrid from the grid. The DG units are now the sole power sources left to regulate the loads. In the case when the generation capacity of the microgenerators is unable to meet the total load demand, the flexible AC distribution system device transits to operate in the emergency mode and functions to momentarily provide for the shortage in real and reactive power.

III. Flexible AC Distribution System Device Model

The single-phase representation of the smart distribution network device is shown in Fig. 2 [12]. The distribution grid

This research work was supported by the School of Electrical and Electronic Engineering, Nanyang Technological University, Singapore, and was also supported by A*STAR under the Smart Grid Project (SERC Grant No.: 112 120 2022) (e-mail: eplso@ntu.edu.sg).

978-1-4673-1943-0/12/$31.00 ©2012 IEEE

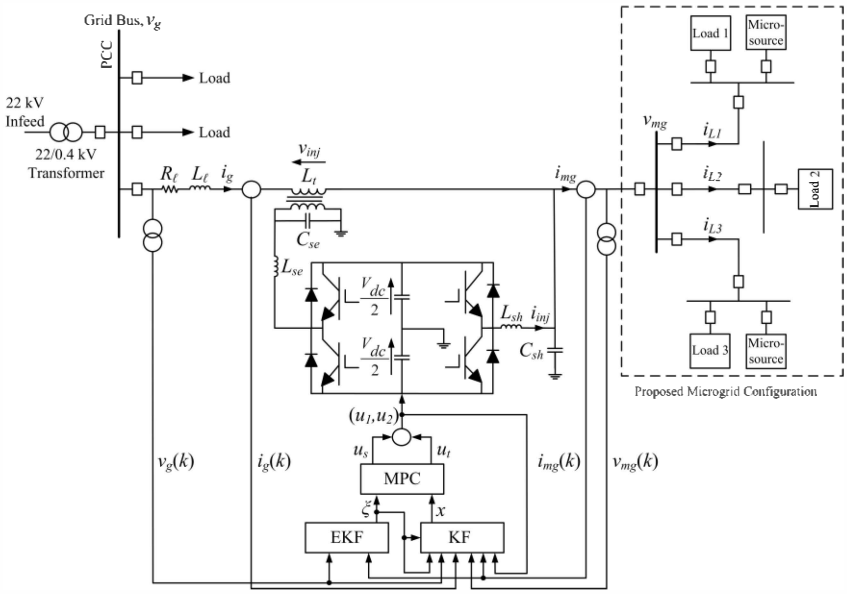

Fig. 1. Overall configuration of the proposed smart distribution network device and the microgrid architecture with EKF denoting the extended Kalman filter and KF denoting the Kalman filter for the plant.

voltage at the PCC and the total current drawn by the microgrid are modeled as v_g and i_{mg} respectively. With the proliferation of power electronics equipment being connected to the distribution grid and the microgrid, both v_g and i_{mg} could be distorted due to the presence of harmonic components. Therefore, v_g is modeled as a source consisting of its fundamental v_f and harmonic v_h that can be represented by

$$v_g = v_f + v_h = V_f \sin(\omega t) + \sum_{h=3,5,\ldots}^{N} V_h \sin(h\omega t - \theta_h) \tag{1}$$

where v_f is the fundamental component of v_g with its peak amplitude V_f and v_h is a combination of the harmonic components of v_g with its peak amplitude V_h and phase angle θ_h. To compensate for the harmonics in v_g, the series VSI injects a voltage v_{inj} that is given by

$$v_{inj} = v_h - v_z - v_t \tag{2}$$

where v_z is the voltage drop across the line impedance of R_ℓ and L_ℓ, and v_t is the voltage drop across the equivalent leakage reactance L_t of the series-connected transformer. Similarly, i_{mg} is also modeled as two components consisting of fundamental i_f and harmonic i_h with their peak amplitudes I_f and I_h respectively and is represented by

$$\begin{aligned} i_{mg} &= i_f + i_h = I_f \sin(\omega t - \varphi_f) + \sum_{h=3,5,\ldots}^{N} I_h \sin(h\omega t - \varphi_h) \\ &= I_f \sin\omega t \cos\varphi_f - I_f \cos\omega t \sin\varphi_f + \sum_{h=3,5,\ldots}^{N} I_h \sin(h\omega t - \varphi_h) \\ &= i_{f,p} + i_{f,q} + i_h \end{aligned} \tag{3}$$

where φ_f and φ_h are the respective phase angles of the fundamental and harmonic components of i_{mg}, and $i_{f,p}$ and $i_{f,q}$ are the instantaneous fundamental phase and quadrature components of i_{mg}. To achieve unity power factor at the grid side, compensate for the harmonics in the microgrid current and achieve load sharing concurrently, the shunt VSI injects a current i_{inj} that is given by

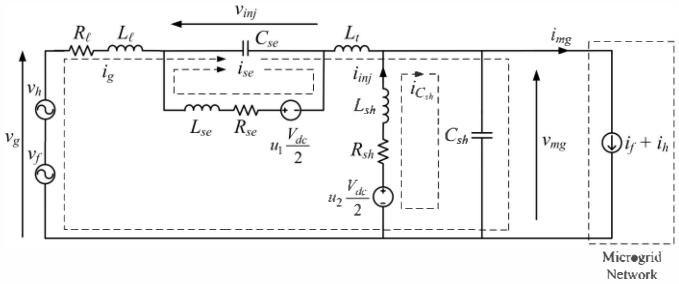

Fig. 2. Single-phase representation of the flexible AC distribution system device.

$$i_{inj} = (i_{f,p} - i_g) + i_{f,q} + i_h + i_{C_{sh}} \tag{4}$$

where i_g is the grid current. The switched voltages across the series and shunt VSIs of the smart distribution network device are represented by $u_1(V_{dc}/2)$ and $u_2(V_{dc}/2)$ respectively. To eliminate the high switching frequency components generated by the series and shunt VSIs, two second-order low-pass interfacing filters which are represented by L_{se}, C_{se}, L_{sh} and C_{sh} are incorporated. The losses of the series and shunt VSIs are modeled as R_{se} and R_{sh} respectively.

To derive a state-space model for the aforementioned system, Kirchhoff's voltage and current laws are applied to the three current loops as shown in Fig. 2.

The following equation is obtained from loop i_g:

$$v_g = i_g R_\ell + (L_\ell + L_t)\frac{di_g}{dt} + v_{inj} + v_{mg} \tag{5}$$

The following equations are obtained from loop i_{se}:

$$\frac{V_{dc}}{2} u_1 = i_{se} R_{se} + L_{se}\frac{di_{se}}{dt} + v_{inj} \tag{6}$$

$$v_{inj} = \frac{1}{C_{se}} \int (i_g + i_{se})\, dt \tag{7}$$

The following equations are obtained from loop i_{Csh}:

$$\frac{V_{dc}}{2}u_2 = i_{inj}R_{sh} + L_{sh}\frac{di_{inj}}{dt} + v_{mg} \tag{8}$$

$$v_{Csh} = \frac{1}{C_{sh}}\int i_{Csh}dt \tag{9}$$

$$i_{mg} = i_g + i_{inj} - i_{Csh} = i_{L1} + i_{L2} + i_{L3} + \ldots + i_{Lk} \tag{10}$$

where k is the number of feeders that are connected to the microgrid. By rearranging (5)–(10), the state-space representation of the system can be obtained as

$$\dot{x} = \overline{A}x + \overline{B}_1 w + \overline{B}_2 u \tag{11}$$

$$y = Cx + D_1 w + D_2 u \tag{12}$$

where

$$\overline{A} = \begin{bmatrix} -\frac{R_\ell}{(L_\ell + L_t)} & 0 & 0 & \frac{1}{(L_\ell + L_t)} & \frac{1}{(L_\ell + L_t)} \\ 0 & -\frac{R_{se}}{L_{se}} & 0 & -\frac{1}{L_{se}} & 0 \\ 0 & 0 & -\frac{R_{sh}}{L_{sh}} & 0 & -\frac{1}{L_{sh}} \\ \frac{1}{C_{se}} & \frac{1}{C_{se}} & 0 & 0 & 0 \\ \frac{1}{C_{sh}} & 0 & \frac{1}{C_{sh}} & 0 & 0 \end{bmatrix}$$

$$\overline{B}_1 = \begin{bmatrix} \frac{1}{L_\ell} & 0 \\ 0 & 0 \\ 0 & 0 \\ 0 & 0 \\ 0 & -\frac{1}{C_{sh}} \end{bmatrix} \quad \overline{B}_2 = \begin{bmatrix} 0 & 0 \\ \frac{V_{dc}}{2L_{se}} & 0 \\ 0 & \frac{V_{dc}}{2L_{sh}} \\ 0 & 0 \\ 0 & 0 \end{bmatrix}$$

$$C = \begin{bmatrix} 0 & 0 & 0 & 0 & 1 \\ 1 & 0 & 0 & 0 & 0 \end{bmatrix} \quad D_1 = \begin{bmatrix} 0 & 0 \\ 0 & 0 \end{bmatrix} \quad D_2 = \begin{bmatrix} 0 & 0 \\ 0 & 0 \end{bmatrix}$$

$x = \begin{bmatrix} i_g & i_{se} & i_{inj} & v_{inj} & v_{Csh} \end{bmatrix}^T$ is the state vector; $u = \begin{bmatrix} u_1 & u_2 \end{bmatrix}^T$ is the control input, with $-1 \le u_k \le 1$, $k = 1,2$; $w = \begin{bmatrix} v_g & i_{mg} \end{bmatrix}^T$ is the periodic exogenous signal; and $y = \begin{bmatrix} v_{mg} & i_g \end{bmatrix}^T$ is the output, which will be regulated to track the desired sinusoidal reference waveforms.

IV. Control Design

With the state-space model presented in Section III, a new MPC algorithm, which extends a recently developed MPC algorithm in [13], is proposed and is specifically designed for fast-sampling systems like our device to track periodic signals. The algorithm decomposes the MPC optimization into two sub-problems: a steady-state sub-problem and a transient sub-problem, which are solved in parallel in different time-scales, thus reducing the computational burdens. However, the MPC algorithm in [13] assumes that the periodic signals have a fixed and known frequency. In this paper, the algorithm is extended to allow an unknown frequency so that it will also be suitable for tracking frequency variations.

In the simulation studies of this paper, the sampling interval is chosen as T_s = 0.2ms, which is considered pretty small in conventional MPC applications, but necessary for the high order of harmonics being tackled for our problem. The state-space model given by (11) and (12) after time-discretization is given by

$$x^+ = Ax + B_1 w + B_2 u \tag{13}$$

$$y = Cx + D_1 w + D_2 u \tag{14}$$

where the subscript + represents the time-shift operator and the exogenous signal w is periodic. It is known that any periodic signal which contains a finite number of harmonics can be written as the output of an autonomous finite dimensional LTI state-space model. For example, if the periodic signal has a fundamental frequency ω and consists of only odd harmonics, the A-matrix of the corresponding state-space model can take a block diagonal form with the blocks given by $\begin{bmatrix} 0 & h\omega \\ -h\omega & 0 \end{bmatrix}$ where $h = 1,3,5,\ldots,$ and the C-matrix $\begin{bmatrix} 1 & 0 & 1 & 0 & \ldots & 1 & 0 \end{bmatrix}$. The initial state of this autonomous model also determines the magnitude and phase angle of this periodic signal. As such, the exogenous signal w in (13) and (14) can be modeled as

$$\dot{\xi} = \overline{A}_\xi(\omega_g, \omega_{mg})\xi \tag{15}$$

$$w = C_w \xi \tag{16}$$

where the matrix $\overline{A}_\xi$ is parameterized by the distribution grid fundamental frequency ω_g and the microgrid fundamental frequency ω_{mg}, both of which should ideally be 50Hz. On the other hand, the desired references that v_{mg} and i_g are to track can be represented by

$$d = \begin{bmatrix} dv_{mg} & di_g \end{bmatrix}^T = C_d \xi \tag{17}$$

To accomplish the goals specified in Section I, dv_{mg} should be regulated to a pure sine wave with a fixed magnitude. For any sags or swells that might occur in v_g, dv_{mg} is decoupled from v_g after an initialization period so that the voltage deviation will not affect v_{mg}. The reference di_g is calculated from the amount of real and reactive power that is drawn from the distribution grid.

The state-space model given by (15)–(17) is known as the exogenous system. The exogenous state ξ, which represents the sets of Fourier coefficients of w and d, can be identified automatically using a Kalman-based linear observer from the signal w being measured and the reference d being specified, provided that the fundamental frequencies ω_g and ω_{mg} are both fixed and known. In our consideration, however, we assume that ω_{mg} is always desired to be 50Hz whereas the distribution grid frequency ω_g may be subjected to slight but unknown variations, which needs to be estimated from the measurement of v_g. To achieve this, an augmented model of (15)–(17) in its discrete-time form is employed by

$$\xi^+ = A_\xi(\omega_g, \omega_{mg})\xi = e^{\overline{A}_\xi(\omega_g, \omega_{mg})T_s}\xi \tag{18}$$

$$\omega_g^+ = \omega_g \tag{19}$$

$$w = C_w \xi \tag{20}$$

$$d = C_d \xi \tag{21}$$

This formulation treats the unknown parameter ω_g as a fixed but unknown state-component that is required to be estimated too. As the augmented model (18)–(21) is now nonlinear, an extended Kalman filter (EKF) is proposed to estimate ξ and identify ω_g simultaneously. It should be noted that the operation of EKF is based on linearization, which is only local and since ω_g may vary, it is known to be close to 50Hz.

In what follows, the control u in (13) and (14) is decomposed into a steady-state control u_s and a transient control u_t as

$$u = u_s + u_t \tag{22}$$

such that $u \to u_s$ and $u_t \to 0$ as $t \to \infty$. Both u_s and u_t will employ a MPC strategy, but the former will adopt a dynamic MPC policy whereas the latter will adopt a more conventional finite-horizon approach. More details of the decomposition and a complete analysis of this MPC strategy can be found in [13]. By letting $x \to x_s$ and $y \to y_s$ as $t \to \infty$ and $u \to u_s$ during steady-state operation, then according to (13) and (14), u_s, x_t and y_s should become

$$x_s^+ = Ax_s + B_1 w + B_2 u_s \tag{23}$$

$$y_s = Cx_s + D_1 w + D_2 u_s \tag{24}$$

subject to the constraint that

$$|u_s| \le 1 \tag{25}$$

u_s is then being generated from a dynamic MPC policy as follows:

$$\hat{\xi}^+ = A_{\hat{\xi}}(\omega_g, \omega_{mg})\hat{\xi} \tag{26}$$

$$u_s = C_{\hat{\xi}}(\omega_g, \omega_{mg})\hat{\xi} \tag{27}$$

where the matrices $A_{\hat{\xi}}$ and $C_{\hat{\xi}}$ are designed offline but the states $\hat{\xi}$ will be optimized online to minimize a quadratic penalty on the tracking error $e_s = y_s - d$, which is a linear function of the exogenous state ξ and the controller state $\hat{\xi}$, in a receding horizon fashion.

The transient signals, which can be defined by $u_t = u - u_s$, $x_t = x - x_s$ and $y_t = y - y_s$ should then satisfy

$$x_t^+ = Ax_t + B_2 u_t \tag{28}$$

$$y_t = Cx_t + D_2 u_t \tag{29}$$

according to (13) and (14), and (23) and (24). In this transient sub-problem, the objective is to make $y_t \to 0$ as fast as possible, subject to the constraint

$$|u_s + u_t| \le 1 \tag{30}$$

A conventional approach of MPC that employs a finite horizon with a terminal cost can be adopted.

It should be noted that frequency variation does not affect the transient sub-problem. The information that it requires includes u_s and x_s, which will be provided by the solution of the steady-state sub-problem, and the plant state x, which can be estimated using a plant Kalman filter. The overall configuration of the proposed control strategy combining the steady-state control u_s and the transient control u_t is shown in Fig. 3.

V. Simulation Studies

The proposed device is tested under different case scenarios using Matlab/Simulink to evaluate its capability to improve the power quality and reliability of the distribution network that the microgrid is connected to. Different types of loads consisting of linear and nonlinear loads for the microgrid are considered in these test cases. For load 1, a 15kVA three-phase PWM adjustable speed drive (ASD) is used. Load 2 is made up of a three-phase linear load and load 3 consists of a three-phase dimmer load which is nonlinear in nature. The per-phase currents i_{L1}, i_{L2} and i_{L3} drawn by the feeders 1, 2 and 3 are shown in Fig. 4. The system parameters are given in Table I. The impedance of the distribution line has been obtained based on the details presented in [14]. The inverter loss resistance of the device has been coarsely estimated because it is not precisely known in practice.

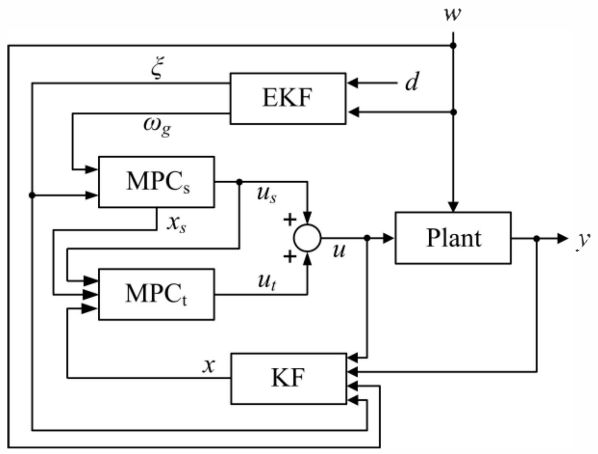

Fig. 3. Overall MPC controller for the flexible AC distribution system device.

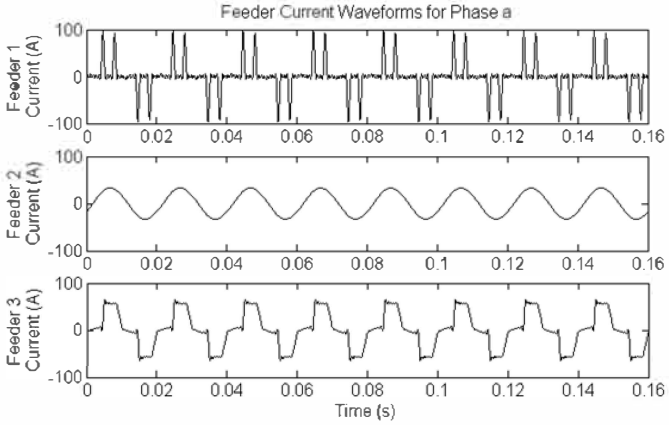

Fig. 4. Per-phase currents drawn by feeders 1, 2 and 3.

TABLE I
PARAMETERS OF THE PROPOSED SYSTEM

Parameter	Value
Distribution grid voltage	v_g = 230V (peak)
DC link voltage	V_{dc} = 800Vdc
Distribution line impedance	R_ℓ = 0.0075Ω, L_ℓ = 25.7μH
Series inductance	L_{se} = 5.0mH
Series capacitance	C_{se} = 10μF
Series loss resistance	R_{se} = 0.01Ω
Shunt inductance	L_{sh} = 1.2mH
Shunt capacitance	C_{sh} = 20μF
Shunt loss resistance	R_{sh} = 0.01Ω
Transformer leakage inductance	L_t = 50μH

A. Test Case 1: Harmonic Compensation and Power Factor Correction during Steady-State Performance with Load Sharing

The first test case demonstrates the capability of the smart distribution network device to perform harmonic compensation for v_g (due to nonlinear loads connected to the grid bus) and i_{mg} (due to the nonlinear loads connected to the microgrid) as well as power factor correction during steady-state operation. The device is also controlled to deliver real power to the microgrid during peak periods when the cost of generation from the grid is high. By doing so, the power required from the grid is reduced and peak shaving is achieved. As such, the device is tasked to deliver 20% and 40% of the real power to the microgrid for 0≤t<0.16s and 0.16≤t<0.32s respectively, while the grid delivers 80% and 60% of the real power to the microgrid.

The voltage and current waveforms under this test case are shown in Figs. 5(a) and 5(b) respectively. The unsteady measurements in microgrid voltage v_{mg} and grid current i_g as shown in the bottom waveforms of Figs. 5(a) and 5(b) during initialization for 0≤t<0.06s is because the controller needs a period of 3 cycles to track the generated references. During steady-state operation, the total harmonic distortion (THD) values of v_g and i_{mg} are 18.39% and 42.1% respectively. With the device injecting the voltage and current harmonics as shown in the middle waveforms of Fig. 5(a) and 5(b), the THD values of v_{mg} and i_g are improved to about 1.5% and 0.4% respectively as shown in the bottom waveforms of Figs. 5(a) and 5(b). The drop in i_g as observed in Fig. 5(b) (bottom) for 0.16≤t<0.32s is due to the decrease in real power delivered by the grid. To achieve power factor correction at the grid side, the device is also controlled to provide the reactive component $i_{f,1}$ of the current i_{mg} as given in (4). A closed-up waveform for v_{mg} and i_g for 0.1≤t<0.14s is shown in Fig. 5(c). It can be observed that the waveform of i_g is in phase with that of v_{mg} to achieve power factor correction.

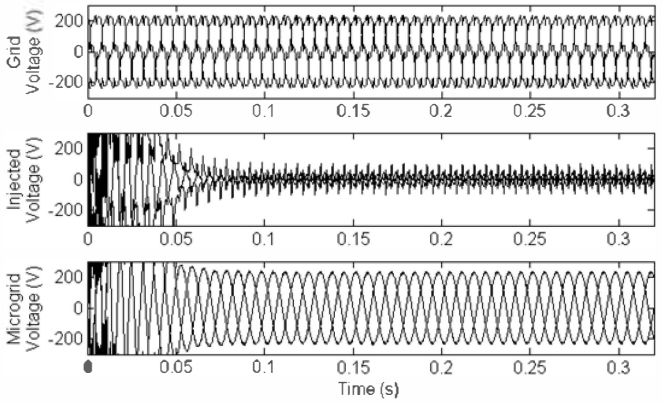

Fig. 5(a). Grid voltage v_g (top), injected voltage v_{inj} (middle) and microgrid voltage v_{mg} (bottom).

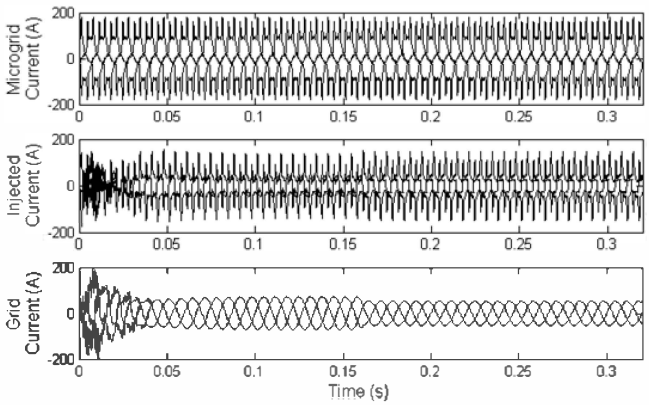

Fig. 5(b). Microgrid current i_{mg} (top), injected current i_{inj} (middle) and grid current i_g (bottom).

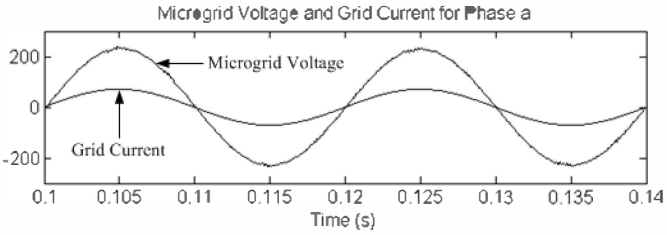

Fig. 5(c). Waveforms of microgrid voltage v_{mg} and grid current i_g .

B. Test Case 2: Voltage and Frequency Variations in the Grid Voltage

In the second test case, the smart distribution network device is controlled to cope with both voltage and frequency variations in the grid voltage v_g. In this test case, the real and reactive power required by the microgrid is kept constant and two operating scenarios are presented.

The first scenario begins with v_g operating at a voltage of 230V. For 0.16≤t<0.32s, a 30% sag in the v_g is simulated and the sag is then clear at t=0.32s. The voltage waveforms of v_g and v_{mg} for 0≤t<0.48s under this case scenario are shown in Fig. 6(a). It is observed that the microgrid voltage v_{mg} can still be regulated at the desired waveform and remains undistorted even though the sag causes a transient in v_{mg} which lasts for about 3 cycles. It also automatically increases di_g in order to gradually restore the power that the grid was initially supplying before the occurrence of the sag. As the controller requires i_g to track di_g, an increase in i_g for 0.16≤t<0.32s is observed in the current waveform in Fig. 6(b) until the sag is cleared at t=0.32s. When the sag has been cleared at t=0.32s, i_g

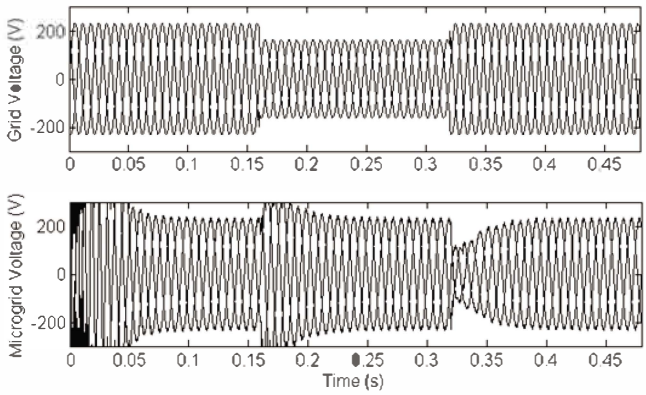

Fig. 6(a). Grid voltage v_g (top) and microgrid voltage v_{mg} (bottom) during grid voltage sag.

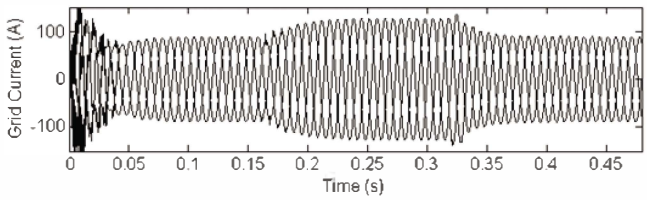

Fig. 6(b). Grid current i_g during grid voltage sag.

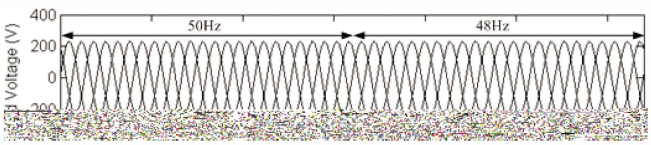

Fig. 10(a). Grid voltage v_g (top) and microgrid voltage v_{mg} (bottom) when the frequency of grid voltage drops to 48Hz.

is adjusted again to restore the grid power as observed in Fig. 6(b).

In the second scenario, the ability to handle slight frequency variations in the grid voltage is demonstrated. The test scenario begins with v_g operating at 50Hz and is then being decreased to 48Hz for $0.16 \leq t < 0.32$s. The voltage waveforms under this scenario are shown in Fig. 7. It should be noted that the device functions to maintain microgrid voltage v_{mg} at 50Hz and at the same time ensures that the frequency variation in grid voltage v_g does not cause any phase shift in v_{mg}. It is observed that the frequency variation in v_g only cause a momentary disturbance to v_{mg} which lasts for less than half a cycle and is regulated to its initial operating frequency of 50Hz. This is achieved as the effect of slight frequency variations has been included in the augmented exogenous model of (18)–(21).

VI. Conclusion

This paper presents a smart distribution network device for a microgrid during both grid-connected and islanded operations. The proposed solution integrates Kalman filters in the control design to identify the required signals for monitoring purposes as well as to extract the harmonic spectra of the grid voltage and the load currents. The device is installed at the PCC that the microgrid and other electrical networks are connected to and is designed to tackle a wide range of PQ issues. It also operates like a DG unit to perform load sharing when the cost of generation from the grid is high to achieve peak shaving. The device is tested under different case scenarios and the results obtained have verified that the device is capable of handling different PQ issues, thus increasing the overall power quality and reliability of the microgrid. However, the proposed design concept still needs further validation by experimental studies. The simulation results obtained in this paper serve as a fundamental step towards the design of control circuits for hardware implementation of the smart distribution network device in the future.

References

[1] R. Lasseter, J. Eto, B. Schenkman, J. Stevens, H. Vollkommer, D. Klapp, E. Linton, H. Hurtado, and J. Roy, "Certs microgrid laboratory test bed, and smart loads," *IEEE Trans. Power Delivery*, vol. 26, no. 1, pp. 325–332, Jan. 2011.

[2] A. Chambers, S. Hamilton, and B. Schnoor, *Distributed Generation: A Nontechnical Guide*. USA: PennWell, 2001.

[3] A. Luo, Z. Shuai, W. Zhu, and Z. J. Shen "Combined system for harmonic suppression and reactive power compensation," *IEEE Trans. Ind. Electron.*, vol. 56, no. 2, pp. 418-428, Feb. 2009.

[4] C. Lascu, L. Asiminoaei, I. Boldea, and F. Blaabjerg, "Frequency response analysis of current controllers for selective harmonic compensation in active power filters," *IEEE Trans. Ind. Electron.*, vol. 56, no. 2, pp. 337-347, Feb. 2009.

[5] L. H. Tey, P. L. So, and Y. C. Chu. "Improvement of power quality using adaptive shunt active filter," *IEEE Trans. Power Del.*, vol. 20, no. 2, pp. 1558-1568, Apr. 2005.

[6] A. Nasiri, Z. Nie, S. B. Bekiarov, and A. Emadi, "An on-line UPS system with power factor correction and electric isolation using BIFRED converter," *IEEE Trans. Ind. Electron.*, vol. 55, no. 2, pp. 722-730, Feb. 2008.

[7] K. S. Low and R. Cao, "Model predictive control of parallel-connected inverters for uninterruptible power supplies," *IEEE Trans. Ind. Electron.*, vol. 55, no. 8, pp. 2844-2853, Aug. 2008.

[8] M. Pascal, G. Garcerá, E. Figueres, and F. G. Espín, "Robust model-following control of parallel UPS single-phase inverters," *IEEE Trans. Ind. Electron.*, vol. 55, no. 8, pp. 2870-2883, Aug. 2008.

[9] A. Gosh, A. K. Jindal, and A. Joshi, "Design of a capacitor-supported dynamic voltage restorer (DVR) for unbalanced and distorted loads," *IEEE Trans. Power Del.*, vol. 19, no. 1, pp. 405-413, Jan. 2004.

[10] D. M. Vilathagamuwa, H. M. Wijekoon, and S. S. Choi, "A novel technique to compensate voltage sags in multiline distribution system–The interline dynamic voltage restorer," *IEEE Trans. Ind. Electron.*, vol. 54, no. 4, pp. 2249-2261, Aug. 2007.

[11] K. H. Kwan, Y. C. Chu, and P. L. So, "Model-based H∞ control of a unified power quality conditioner," *IEEE Trans. Ind. Electron.*, vol. 56, no. 7, pp. 2493-2502, Jul. 2009.

[12] A. Gosh and G. Ledwich, *Power Quality Enhancement Using Custom Power Devices.* Norwell, MA: Kluwer, 2002, pp. 380-406.

[13] Y. C. Chu and M. Z. Q. Chen, "Efficient model predictive algorithms for tracking of periodic signals," *Journal of Control Science and Engineering*, vol. 2012, Article ID 729748, 13 pages, 2012. doi:10.1155/2012/729748.

[14] C. Y. Teo, Principles and Design of Low Voltage Systems. Singapore: Byte Power Publications, 1997.